[4]Cyclo-N-ethyl-2,7-carbazole Synthesis, structural, electronic and charge transport properties

Fabien Lucas, Lambert Sicard, Olivier Jeannin, Joëlle Rault-Berthelot, Emmanuel Jacques, Cassandre Quinton, Cyril Poriel

10.1002/chem.201901066

WILEY-VCH

DOI: 10.1002/ ((please add manuscript number))

Article type: Full Paper

[4]Cyclo-*N*-ethyl-2,7-carbazole: Synthesis, structural, electronic and charge transport properties

*Fabien Lucas,[a] Lambert Sicard,[a] Olivier Jeannin,[a] Joëlle Rault-Berthelot,[a] Emmanuel Jacques,[b] Cassandre Quinton,[a] Cyril Poriel[a]**

[a] *Univ Rennes, CNRS, ISCR-UMR CNRS 6226, F-35000 Rennes, France*

email: cyril.poriel@univ-rennes1.fr

[b] *Univ Rennes, CNRS, IETR-UMR 6164, F-35000 Rennes, France*

Keywords: nanoring, organic field effect transistor, organic semiconductor, charge transport, bridged cyclo-oligophenylenes, structure-properties relationship

Abstract

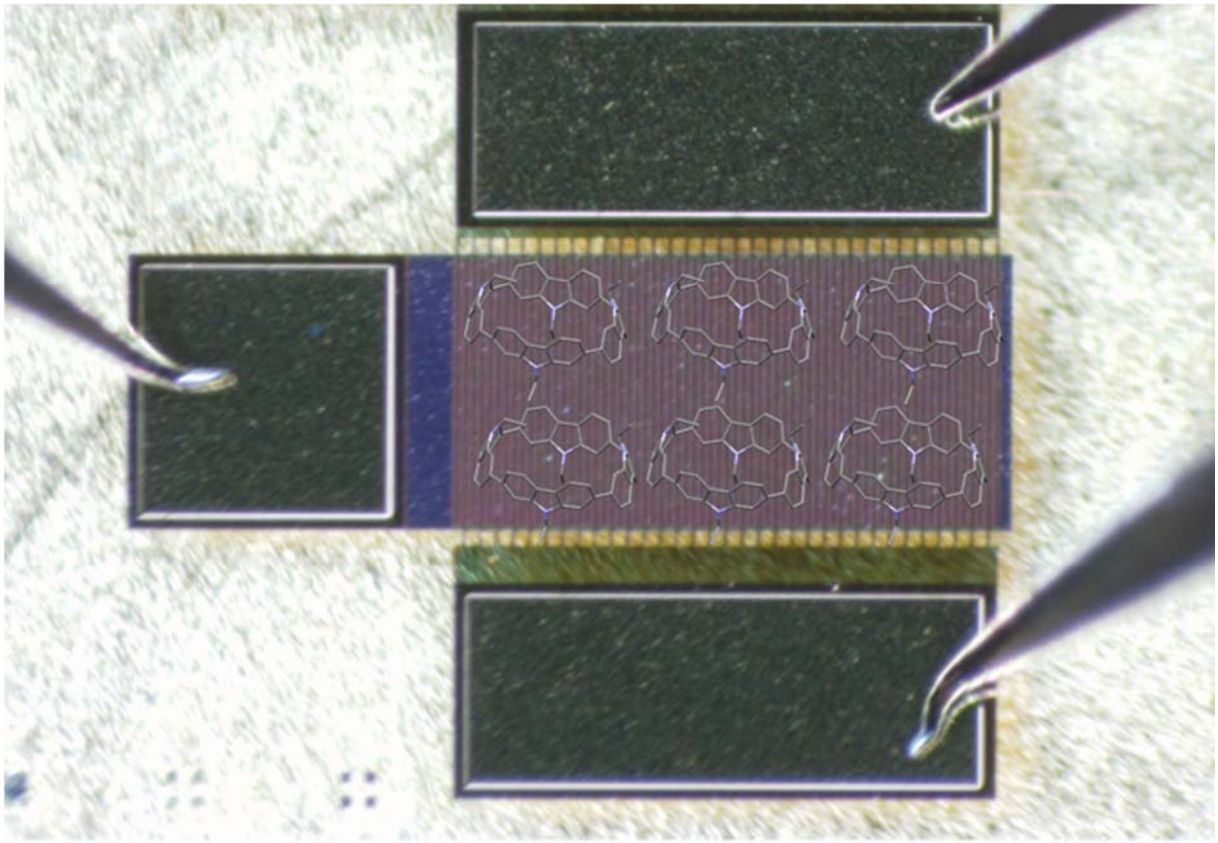

Nanorings, which are macrocycles possessing radially directed π-orbitals have shown a fantastic development in the last ten years. Unravelling their unusual electronic properties has been one of the driving forces of this research field. However, and despite promising properties,

their incorporation in organic electronic devices remain very scarce. In the present work, we aim to contribute to bridge the gap between organic electronic and nanorings by reporting the synthesis, the structural and electronic properties and the incorporation in an Organic Field Effect Transistor (OFET) of a cyclic tetracarbazole, namely [4]cyclo-*N*-ethyl-2,7-carbazole (**[4]C-Et-Cbz**). The structural, photophysical and electrochemical properties have been compared to those of structurally related analogues [4]cyclo-9,9-diethyl-2,7-fluorene **[4]C-diEt-CF** (with carbon bridges) and [8]-cycloparaphenylene **[8]CPP** (without any bridge) in order to shed light on the impact of the bridging in nanorings. This work shows that nanorings can be used as an active layer in an OFET and provides a first benchmark in term of OFET characteristics for this type of molecules.

Introduction

With the synthesis of the first cyclo-*para*-phenylene (CPP) in 2008,[1] hoop-shaped π-conjugated macrocycles possessing radially directed π-orbitals (so called nanorings or nanohoops) have been the subjects of intense research worldwide.[2-6] Compared to their linear counterparts, nanorings present singular electronic and structural characteristics.[3-7] In addition, studies of the influence of the nanoring size and of the building units on the structural, electronic, physical, chiral and encapsulating properties have already shown the diversity of this field.[3-8] The growing interest in nanorings chemistry and physics has led to recent applications such as imaging tools in biology[9] or complexation of single-walled carbon nanotubes.[10] In 2016, Nuckolls and coworkers have shown the several advantages of cyclic oligomers over corresponding linear counterparts in electronics devices.[11] In 2019, theoretical calculations have predicted the strong potential of CPPs and Donor-Acceptor CPPs as high mobility materials.[12, 13] However, and despite the fantastic development of organic electronics technology in the last twenty years,[14] only very few examples of nanorings incorporation in

organic electronic devices have been reported so far.[15, 16] Bridging the gap between organic electronics and nanorings appears hence as an appealing challenge. In this context of organic electronics, mobility of charge carriers is a central concept,[17] which drives the performance of the three types of devices, namely Organic Light-Emitting Diode (OLED), Organic Field-Effect Transistor OFET and solar cell. However, the charge transport properties of nanorings are almost unknown and the literature only reports one example of a nanoring, namely 10-cycloparaphenylene (**10[CPP]**), for which an electron mobility value of 4.5×10^{-6} cm^2 V^{-1} s^{-1} has been measured in an electron-only device using space charge limited current technique (SCLC).[16] In order to further incorporate nanorings in efficient electronic devices in the future, knowledge of their charge carriers motilities is a mandatory step. As far as we know, no example of a nanoring in an OFET has ever been reported. In the present work, we report the synthesis, the electronic properties and the incorporation in an OFET of a cyclic tetracarbazole linked at *para* positions C2 and C7, namely [4]cyclo-*N*-ethyl-2,7-carbazole (**[4]C-Et-Cbz**). The structural, photophysical and electrochemical properties have notably been compared to those of structurally related analogues [4]cyclo-9,9-diethyl-2,7-fluorene **[4]C-diEt-CF** (with carbon bridges) and [8]-cycloparaphenylene **[8]CPP** (without any bridge, see molecular structures in chart S1) in order to shed light on the impact of the bridging in nanorings. OFET characterization of **[4]C-Et-Cbz** provides a hole mobility μ_{FE} of 1.1×10^{-5} cm^2 $V^{-1}s^{-1}$, a threshold voltage V_{TH} of 24 V, a subthreshold swing SS of 2.2 V/dec and an on/off ratio of the drain current (I_{Don}/I_{Doff}) of $4.26\ 10^4$. This work not only shows that nanorings can be used as active layer in OFETs but also provides the first OFET characteristics benchmark for nanorings.

Results and discussion

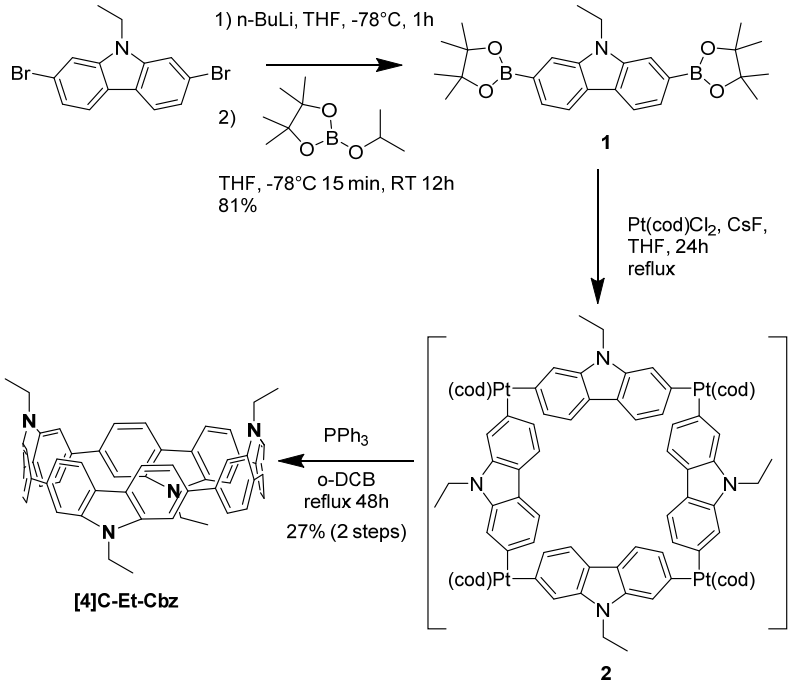

Scheme 1. Synthesis of **[4]C-Et-Cbz**

The carbazole as its 'all carbon' structural analogue fluorene belongs to the family of 'bridged biphenyls', which are both key building units in the design of organic semi-conductors for electronics.[18-22] In linear organic semi-conductors, the bridge has a significant impact on the structural properties (by notably rigidifying and flattening the molecular structure) which in turn modify the electronic properties.[20, 23-25] In the case of carbazole, the effect of the nitrogen bridge is strong. For example, this fragment displays an electron-rich character, which has been advantageously used for hole transport in organic semi-conductors. However, in nanorings, these effects have not been described to date. In 2006, Müllen and coworkers have reported a cyclododeca-2,7-carbazole around a porphyrin template.[26] The first examples of highly strained 2,7-cyclocarbazoles possessing a radial π-conjugation have only been reported ten years later, in 2016, by Yamago and coworkers.[27] These molecules, constituted of four carbazole units substituted on the nitrogen atoms by either a methyl or a phenyl group, were designed to investigate the inner region of nanorings by ^{1}H NMR studies and their electronic properties, despite being recorded, were not discussed.

The synthetic pathway to **[4]C-Et-Cbz** reported herein is inspired by the works of Yamago and coworkers[28] and Isobe and coworkers (Scheme 1).[29] On first attempt, **[4]C-Et-Cbz** was obtained with a relatively low yield of 6% from the di-pinacolborane carbazole **1** in two steps (1. $Pt(cod)Cl_2$/CsF at the reflux of THF for 24h, 2. $P(Ph)_3$ in toluene 30 min at rt and then 24h at 100°C, Table S1). This yield is half of that reached in the case of its structurally related tetracyclofluorene analogue [4]cyclo-9,9-diethyl-2,7-fluorene **[4]C-diEt-F** (12%), under strictly identical conditions.[30] As the synthesis of nanorings is a central point in the field and particularly if an electronic application is envisaged, synthetic investigations (scouting the impact of temperature, solvent and reaction time, see Table S1) for both the transmetallation and reductive elimination steps were performed. The best conditions (Scheme 1) found are described below. The intermediate **2**, based on four square-shaped tetranuclear platinum complexes, was obtained by stirring the dipinacol carbazole **1** with $Pt(cod)Cl_2$ and cesium fluoride in a refluxing THF solution for 24 h. Then, the carefully dried crude containing **2** was treated with triphenylphosphine in *o*-dichlorobenzene, 1 h at rt and 48 h at 180°C to give **[4]C-Et-Cbz** with an improved yield of 27% from the dipinacolborane carbazole **1**. Thus, the reductive eliminations step being unfavoured because of the strain energy, it can be helped by increasing both the temperature (by using *o*-dichlorobenzene as previously reported by Isobe and coworkers for cyclonaphthylene nanohoops[31]) and reaction time. Calculations of the strain energy of **[4]C-Et-Cbz** (73 $kcal.mol^{-1}$, see SI for details on calculations, Figure S15) appears almost identical to that previously described for **[4]C-diEt-F** (72.4 $kcal.mol^{-1}$),[30] showing the similar impact of the C and N bridge (substituted herein with ethyl chains) on this parameter. In the end, the global yield of the formation of **[4]C-Et-Cbz** from its corresponding dibromocarbazole (ca 22%) has been increased threefold using the present optimized conditions compared to that described by Yamago and coworkers *via* a distanylated carbazole (yield of

7% for a N-methyl-substituted cyclocarbazole).[27] This is an interesting feature for the future incorporation of nanorings in electronic devices.

The ^{1}H NMR of **[4]C-Et-Cbz** displays in the aromatic region an upfield shifted singlet corresponding to the hydrogen atom H^1 (δ=6.51 ppm) and two deshielded signals assigned by 2D NMR spectroscopy to H^3 (δ=7.49 ppm) and H^4 (δ=7.92 ppm), Figure 1, left. The presence of only three signals for the aromatic region is in accordance with a symmetrical molecule possessing either an αβαβ or an αααα arrangement (relative position of the nitrogen bridges). A NOESY experiment allows to discriminate between the two rotamers exclusively showing the through-space coupling between protons H^1 and H^3 (Figure 1, right). This indicates that we are in presence of the all anti conformer αβαβ. As the αβαβ conformer was also obtained following the same approach in the case of the fluorene analogue **[4]C-diEt-F**,[30] this result indicates that the nature of the bridge (N *vs* C) does not modify the formed rotamer. The variable-temperature NMR studies from 223 K to 373 K do not show any significant modifications of the ^{1}H spectrum (Figures S5 and S10), confirming the presence of a single isomer, and not a time-averaged dynamic structure, at room temperature. These variable temperature NMR studies also indicate that the carbazole units cannot flip and that the other rotamers (αααβ, αααα and ααββ isomers) cannot be obtained by thermal input (until 373 K)

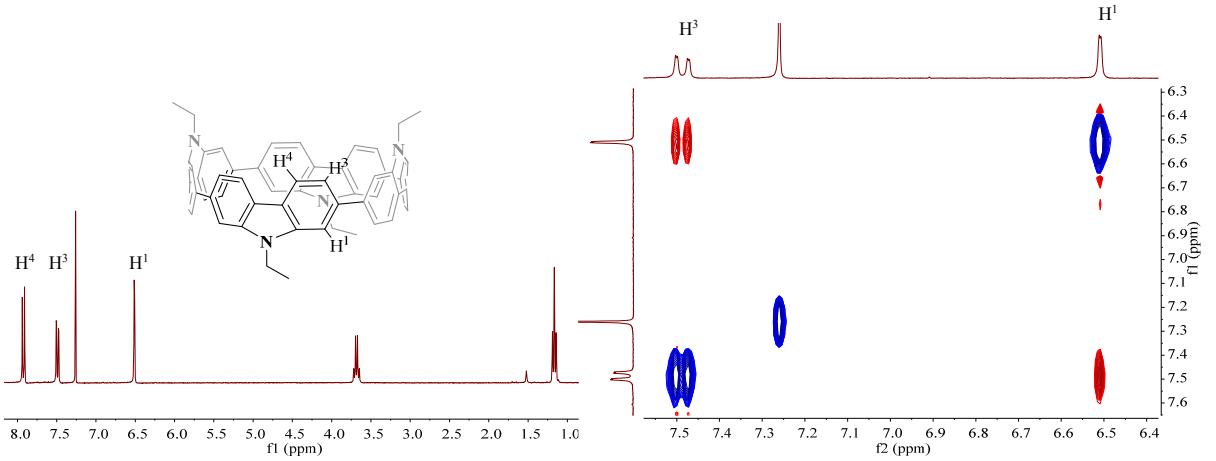

Figure 1. Left: ^{1}H NMR spectrum of **[4]C-Et-Cbz** in $CDCl_3$. Right: selected part of the NOESY spectrum in $CDCl_3$ showing the H^1 /H^3 through space correlation (full spectra can be found in the SI, Figure S42).

As exposed above, the hydrogen atom H^1 appears to be the most shielded due to the ring current of the macrocyle to which it is exposed.[27] It suggests the carbazole units are tilted the bridge side towards the inside of the ring (as also observed in single-crystal X-Ray crystallography, see below). The degree of tilt of the two other [4]-cyclocarbazoles[27] reported in literature (substituted on the nitrogen atom by either methyl or phenyl units) seems to be the same since they display similar H^1 chemical shifts of 6.45-6.51 ppm in ^{1}H NMR. Thus, in the case of the [4]-cyclocarbazole family, the size of the pending substituent seems to have no influence on the arrangement of the nanoring in solution, unlike recent results reported for the [4]-cyclofluorene family.[30]

X-Ray diffraction of single crystals of **[4]C-Et-Cbz** (Figure 2), which were obtained by vapor diffusion of hexane in a concentrated solution of chloroform, confirms the *αβαβ* conformation assigned by NMR. **[4]C-Et-Cbz** crystallizes in a C2/c group and the length of the C/C bonds of the carbazole units (around 1.40 Å) indicates that the benzenoid character is reasonably conserved, such as its non-bridged analogue **[8]CPP** as reported by Jasti and coworkers (CCDC reference : 871414).[32] **[4]C-Et-Cbz** forms a distorted ellipsoidal nanoring with axes of 11.1 and 10.6 Å Figure 2, top-right), which is different than its fluorene analogue **[4]C-diEt-F**, which forms a perfect circle (diameter=11.0 Å, CCDC reference:1580867).[30] As shown in the

NMR part, X-ray diffraction confirms that the upper part of each carbazole (including the nitrogen atom) is tilted towards the centre of the nanoring. The shortest distance between two cofacial hydrogen atoms is hence measured between the two H^1 atoms (mean distance H^1-H^1: 8.05 Å, Figure S16). Then, the corresponding distance between two cofacial hydrogen atoms gradually increases from H^3-H^3 (mean distance: 10.15 Å, Figure S17) to H^4-H^4 (mean distance: 11.87 Å, Figure S18). Due to this inclination, the cofacial nitrogen atoms are also relatively close to each others, $d_{N\text{-}N}$=9.51 and 9.04 Å (Figure 2, top-left). Thus, the solid state molecular arrangement of **[4]C-Et-Cbz** is similar to that found for **[4]C-diEt-F**, with the bridges pointing towards the centre of the ring.

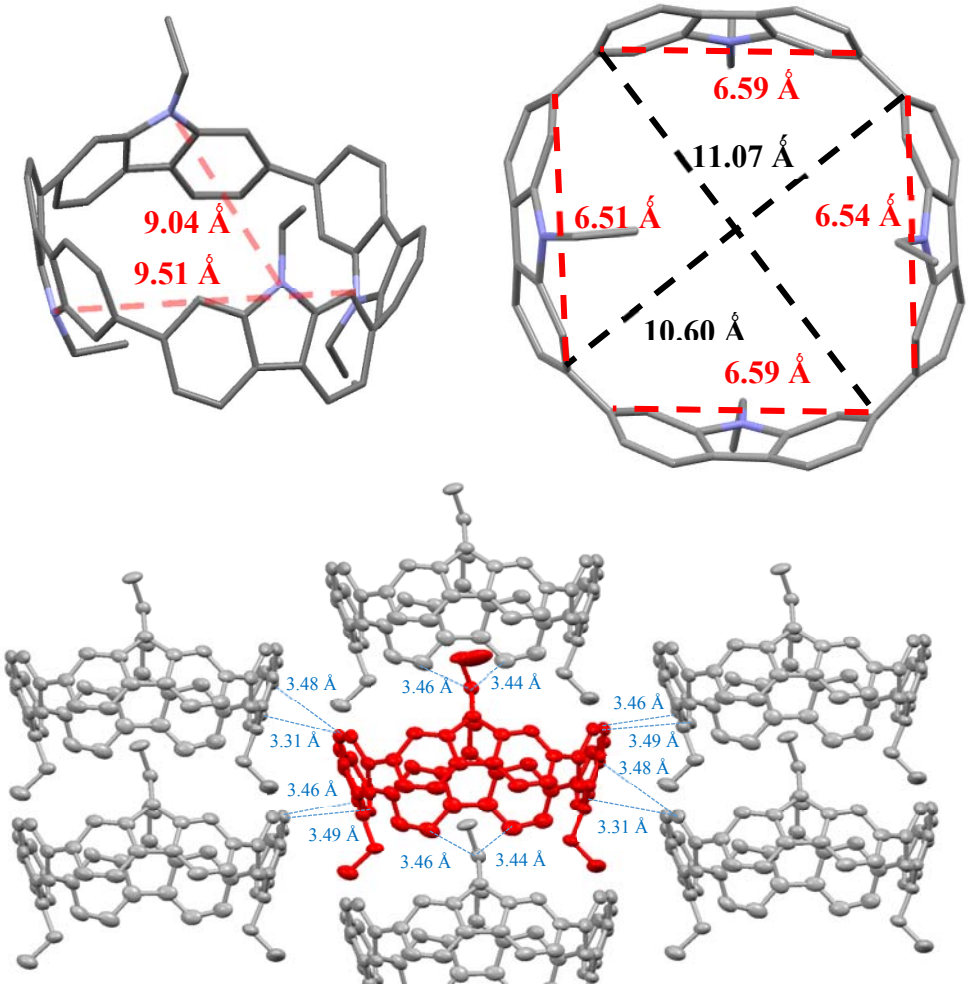

Figure 2. X-Ray crystal structure representations (Top) and packing diagram (Bottom) of **[4]C-Et-Cbz** with distances in Ångström.

As the main factors at the origin of the specific electronic properties of the nanorings are the deformations of the constituted units and their relative arrangement,[7] those of the present cyclocarbazole **[4]C-Et-Cbz** deserve to be precisely stressed out. Four structural parameters should be considered: the out-of-plane distortion, the bending angle, the displacement angle and the torsion angle (see definitions and detailed calculations in SI, Figure S21-S26). First, the distance C2-C7 of a carbazole unit can give an idea of its out-of-plane distortion. For **[4]C-Et-Cbz**, this distance is short (around 6.56 Å, varying from 6.51 to 6.59 Å depending on the carbazole unit, Figure 2-right), clearly showing the strong deformation of the carbazole units when compared to differently substituted carbazoles (the C2-C7 distance is evaluated at around 6.8 Å, Figure S31).[33-35] Furthermore, the bending angle is measured at around 129° for the carbazole units in **[4]C-Et-Cbz** (Table S8), whereas it is found at around 178° (Table S11) for the previously mentioned carbazoles,[33-35] close to planarity (180°). Thus, the short C2-C7 distances and small bending angles measured for **[4]C-Et-Cbz** show the high deformation of the present carbazole fragments. Nevertheless, it is important to note that the mean displacement angle[3] measured for **[4]C-Et-Cbz**, 7.20° (Table S9), is smaller than that of non-bridge analogue **[8]CPP**, 9.58° (Table S10),[32] and almost identical to that of carbon-bridged analogue **[4]C-diEt-F**, 7.10°,[30] showing that the bridge (either carbon atom in fluorene or nitrogen atom in carbazole) tends to flatten the biphenyl unit. In addition, the mean internal torsion angle between two phenyl units of the same bridged biphenyl is small, evaluated around 1.34° (ranging from 0.09° to 2.87°) for **[4]C-Et-Cbz** (Figure S26). This value is higher than that observed in **[4]C-diEt-F** for which the angle is null.[30] Thus, in **[4]C-Et-Cbz**, the presence of a nitrogen bridge between two phenyl rings flattens the structure of the carbazole unit compared to a biphenyl in **[8]CPP** but nevertheless in a less efficient manner than the carbon bridge of **[4]C-diEt-F**. It can be hence concluded that the nitrogen bridge provides more structural flexibility than the carbon bridge in a nanoring constituted of four units. Finally, the

torsion angle between two adjacent carbazole units is also an important parameter as it is notably involved in the stabilization/destabilization of the frontier molecular orbitals.[7] The mean torsion angle appears herein as high as 40.6° (values comprised between 38.38 and 42.35°, Figure S24), which is similar to that measured in **[4]C-diEt-F** (41.5° between two fluorene units)[30] and significantly higher than that of **[8]CPP** (24.3° between two phenyl units, Figure S29).[32] Thus, one can conclude that the presence of a bridge induces higher torsions between the constitutive units than in non-bridged CPP. To conclude, bridged-oligophenylene nanorings display a strong deformation of the constitutive units and a high torsion between them. These parameters seems to be one of the structural particularities of bridged-oligophenylene nanorings and will have important repercussions in the electronic properties described below.

The packing diagram of **[4]C-diEt-Cbz** shows that the nanorings form a tube-like structure along the b axis and are stacked along the a axis with a particularly short C-C distance of 3.31 Å, inferior to the sum of their van der Waals radii ($d_{C\text{-}C}$=3.4 Å[36], Figure 2-bottom and Figure S27). For a given nanoring (coloured in red in Figure 2-bottom), which is surrounded by six other nanorings, many short C-C distances comprised between 3.31 and 3.49 Å are detected. It should be mentioned that the building unit carbazoles are involved in a different way. Thus, two cofacial carbazole units of each nanoring display short C/C distances with the carbazoles of two other surrounding molecules (from 3.31 to 3.49 Å). The two other cofacial carbazoles are also involved in short contacts but with either its own pending ethyl chain or with the ethyl chain of a surrounding molecule (3.44 and 3.46 Å), showing that the pending chains have a role in the packing diagram. Similar conclusions have been drawn with the ethyl chains borne by the bridges of **[4]C-diEt-F**. This feature could be used in the future to tune the supramolecular arrangement of such nanorings by alkyl chain engineering.

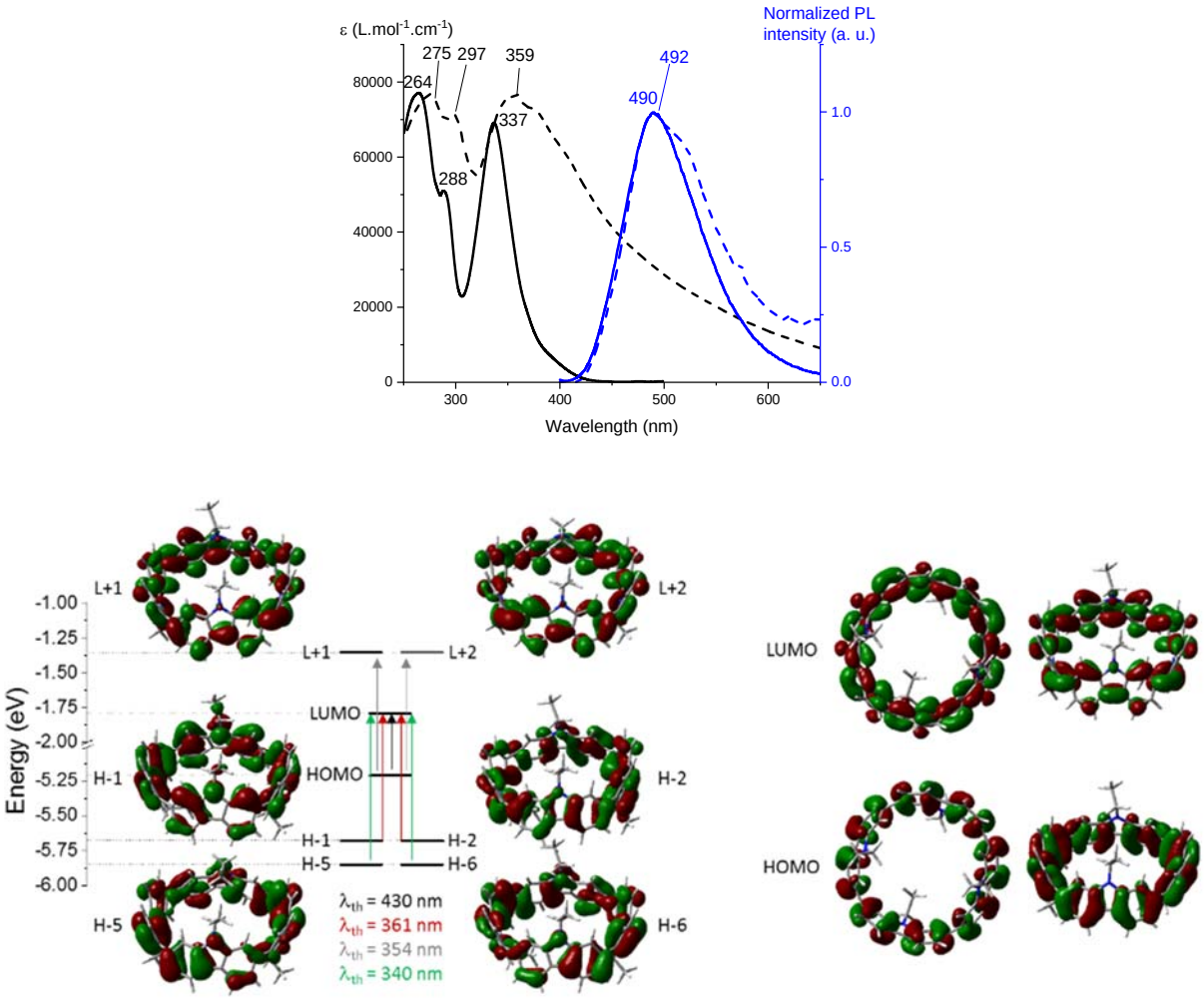

Figure 3. Top: Combined absorbance (black) and emission (blue, λ_{exc} = 336 nm for the solution and 350 nm for the film) spectra of **[4]C-Et-Cbz** in THF (solid lines) and in spin-coated film (obtained from a THF solution, 1 mg/mL, dashed lines). Bottom: Representation of the energy levels and the main molecular orbitals involved in the electronic transitions of **[4]C-Et-Cbz** obtained by TD-DFT B3LYP/6-311+G(d,p), shown with an isovalue of 0.02 [e bohr^{-3}]$^{1/2}$. For clarity purposes, only the major contribution of each transition is shown (see SI for details).

To precisely compare the photophysical properties of **[4]C-Et-Cbz** with those of the two other nanorings of interest in this study, they have been investigated in different solvents, in chloroform (to compare the absorption properties with the ones of **[8]CPP**,[28] see Figure S33), in cyclohexane (to compare the absorption properties with the ones of **[4]C-diEt-F**,[30] see Figure S32) and in THF (to compare the fluorescence properties of the three nanorings,[37] Figure 3 and S34 and S38). The absorption spectra of **[4]C-Et-Cbz** are similar regardless of the solvent ($CHCl_3$, THF or cyclohexane), with absorption maxima at around 264, 288 and 337 nm

(Figure 3, top, black solid line). In addition and as for the two other nanorings, **[8]CPP**[28] and **[4]C-diEt-F**,[30] **[4]C-Et-Cbz** displays a band tail at around 400 nm which is due, according to TD-DFT calculations, to a symmetry forbidden (f=0) HOMO→LUMO transition (Figure 3, bottom). Indeed, as observed for the nanorings in general, the two orbitals are delocalized on the whole nanoring with a radial geometry. On the other hand, the band at around 337 nm is much more intense with a molar absorption coefficient ε of 7×10^4 mol.L^{-1}.cm^{-1}. According to TD-DFT calculations, this band is due to six transitions (almost degenerated two by two): H-1→LUMO and H-2→LUMO (λ_{th}=361 nm), HOMO→L+1 and HOMO→L+2 (λ_{th}=354 nm) and H-5→LUMO and H-6→LUMO (λ_{th}=340 nm). The H-1, H-2, H-5 and H-6 orbitals are all delocalized on the whole nanoring, including the nitrogen atoms, and are thus specific of chromophore **[4]C-Et-Cbz**. However, the HOMO density resembles that of **[8]CPP**,[38, 39] with no participation of the nitrogen atom, whereas the LUMO density resembles the one of the molecule of carbazole **Cbz** itself, with no participation of the carbon atom in *para* position of the nitrogen atom. The L+1 and L+2 orbitals are similar to the ones of **[8]CPP**[39] in the way that they are mainly localized on two opposite carbazole units, but the repartition of the lobes seems specific to **[4]C-Et-Cbz**. Thus, despite the involvement of molecular orbitals specific to **[4]C-Et-Cbz,** the presence and the nature of the bridge seem to have no impact on this absorption band at ca 340 nm which is also observed in **[8]CPP** (λ=340 nm, ε=3×10^4 mol.L^{-1}.cm^{-1} in $CHCl_3$)[28] and in **[4]C-diEt-F** (λ=347 nm, ε=9×10^4 mol.L^{-1}.cm^{-1} in cyclohexane), Table S12.[30] On the other hand, the band observed at 292 nm in cyclohexane for **[4]C-Et-Cbz** is not found for **[8]CPP** nor **[4]C-diEt-F** but is observed in **Cbz** (λ=292 nm in cyclohexane). Note that the molar absorption coefficient of **[4]C-Et-Cbz** at 292 nm (ε=5.7×10^4 mol.L^{-1}.cm^{-1} in cyclohexane) is almost four times the one of **Cbz** (ε=1.6×10^4 mol.L^{-1}.cm^{-1} in cyclohexane) matching with the involvement of four carbazole units. The fourth band, located around 260 nm, also seems specific to **[4]C-Et-Cbz**, inherited from **Cbz** (λ=255 nm, ε = 1.1×10^4 mol.L^{-}

^{1}.cm^{-1}). In summary, the low energy transitions (λ=340 and 400 nm) are also found in **[8]CPP** and **[4]C-diEt-F** (and in nanorings in general) whereas the high energy transitions (λ=290 and 260 nm) are specific of **[4]C-Et-Cbz**.

In emission spectroscopy (Figure 3, top, blue solid line and Figures S32-S38), **[4]C-Et-Cbz** displays an unresolved spectrum (in the three solvents) with a maximum at 490 nm (in THF). The emission spectrum of **[4]C-Et-Cbz** resembles that of **[4]C-diEt-F** (λ_{max}=492 nm in THF, Figure S38) and is highly blue-shifted compared to that of **[8]CPP** (533 nm in THF).[37] Thus, the presence of a bridge linking two phenyl units (in both **[4]C-Et-Cbz** and **[4]C-diEt-F**) leads to an emission spectrum strongly blue shifted (by 46-48 nm) compared to that of non-bridged **[8]CPP**. As the absorption spectra of **[4]C-Et-Cbz** and **[8]CPP** are similar, this induces a smaller Stokes shift in the former than in the latter. This can be explained by a weaker conjugation because of both a decrease of the displacement angle and an increase of the torsion angle between biphenyl units, such as for larger CPPs.[40] Thus, the emission of bridged cyclo-oligophenylenes occurs in a different range than that of non-bridged analogues and the effect of the bridging is different to that of linear analogues.

Furthermore, the quantum yield of **[4]C-Et-Cbz** in THF is measured at 16% and thus is twice that of **[8]CPP** (8%),[37] which also indicates a bigger partial levelling of the excited state (due to the bridge) which induces an enhanced self-trapping of the exciton and thus a higher transition dipole moment for **[4]C-Et-Cbz** compared to **[8]CPP**.[40] Note that, if the nature of the bridge seems to have no influence on the shape of the spectrum, it impacts the intensity of the fluorescence since the quantum yield measured for **[4]C-diEt-F** in THF is almost twice (28%) the one of **[4]C-Et-Cbz**. The fluorescence decay curve of **[4]C-Et-Cbz** measured in THF (λ_{exc}=310 nm, Figure S37) provides a lifetime of 5.8 ns, which is shorter than that of **[8]CPP** reported at 17.6 ns.[37] The radiative rate constant k_r of **[4]C-Et-Cbz** is calculated to be 2.8×10^{7} s^{-1}, being six times higher than that of **[8]CPP** (4.8×10^{6} s^{-1}), whereas the non-radiative constant

of **[4]C-Et-Cbz** is only three times higher than that of **[8]CPP** (resp. 1.5×10^8 s^{-1} and 5.2×10^7 s^{-1}). Thus, this confirms that the increase of the quantum yield induced by the presence of the bridge (from **[8]CPP** to **[4]C-Et-Cbz**) is due to a higher transition dipole moment. To conclude, in dilute solution, the incorporation of four nitrogen bridges within the **[8]CPP** molecular structure significantly shifts the emission maxima to lower wavelengths and increases the quantum yield.

In thin film (Figure 3, top, dashed lines), the most relevant differences compared to solution are surprisingly observed for the absorption spectra and not for the emission spectra. In absorption, one can note a small red shift and an increase of full width at half maximum of the bands and an important band tail at high wavelengths. In emission, only a small extension of the bandwidth is observed with no shift of the maximum between solution and thin film (λ= 492 nm). This feature allows a high control of the emission wavelength in the solid state, key point for future optoelectronic applications. Furthermore, the absolute quantum yield of thin film of **[4]C-Et-Cbz** was measured at 15%, a value identical to that obtained for the solution of **[4]C-Et-Cbz** in THF (16%). This shows the great stability of the emission in the solid state. It should be noted that this is the first time that a nanoring displays the same quantum yield both in solution and in solid state (for example, the one of **[4]C-diEt-F** is decreased by a factor 2 in thin film compared to solution[30]). To sum up, the emission properties of **[4]C-Et-Cbz** (both shape of spectrum and quantum yield) in diluted solution are kept in spin-coated film. This finding appears appealing for the future design of carbazole nanorings for solid state optoelectronics.

Electrochemical analyses of **[4]C-Et-Cbz** were performed in DMF (for reduction) and in CH_2Cl_2 (for oxidation). Cyclic voltammetry (CV) recorded between 0.0 and -2.65 V presents two irreversible reduction waves with two maxima (or shoulder) at -2.40 (sh) and -2.55 V *vs* SCE (Figure S39). In oxidation, three successive processes with maxima at 0.86, 1.40, and 2.03 (sh) (*vs* SCE) were recorded (Figure 4, top left). The HOMO and LUMO energies calculated

from the onset potential of the first oxidation and reduction (E_{onset}^{ox}: 0.77 V and E_{onset}^{red}= -2.18 V) were respectively evaluated at -5.17 and -2.22 eV leading to a HOMO/LUMO gap of 2.95 eV. The first oxidation of **[4]C-Et-Cbz** is therefore significantly shifted compared to that of its structurally related cyclofluorene analogue **[4]C-diEt-F** (E_{onset}^{ox}= 0.86 V, HOMO= -5.26 ev).[30] and even more shifted compared to that of **[8]CPP** (E_{onset}^{ox}= 0.93 V, HOMO= -5.33 ev).[41] This feature translates the more electron-rich character of **[4]C-Et-Cbz**. Despite the three molecules being constructed on the cyclic association of eight phenyl units, the different first oxidation potential shows the important role played by the bridge (C *vs* N) on the electrochemical properties (and more precisely herein on the HOMO energy level). One can note that the trend is similar to that of their building units (HOMOs decrease from N-ethylcarbazole[42] to 9,9'diethylfluorene[43] to biphenyl[44]).

When scanning between 0 and 1 V, one can observed (i) that the first wave is not fully reversible and (ii) that there is a slight shift and a current decrease after recurrent sweeps in the same potential range signing the reactivity of the radical cation formed (Figure 4, top right). This instability of **[4]C-Et-Cbz**$^{\cdot+}$ is due to the high reactivity of the C3 and C6 positions of the carbazole units which can rapidly be involved in C-C couplings (see below).[45] The evolution of the CVs is even accentuated when cycling between 0.2 and 1.86 V (Figure 4, bottom left) with a complete disappearance of the first oxidation wave at 0.86 V, in favour of the appearance and the regular growth of a new redox system centred at 1.5/1.3 V and of the covering of the electrode surface with an insoluble deposit. The presence of a deposit on the electrode surface indicates an anodic electrodeposition process. If anodic coupling is a well-known technique to generate π-conjugated oligomers and polymers from various linear building blocks, [46][51, 52] as far as we know, this strategy has never been examined for nanorings. In the present case, this anodic coupling seems to be efficient as at the tenth scan, the current intensity at 1.5 V is more than seven times that of the first scan. The electrochemical behaviour of the electrodeposited

material studied in a solution in absence of any electroactive substance (Figure 4, bottom right) shows a reversible redox process with a maximum at 1.5 V and a E_{onset}^{ox} at 1.02 V (HOMO= -5.42 eV). Thus, there is surprisingly a HOMO energy level lowering of 0.25 eV (from -5.17 to -5.42 eV) between the monomer **[4]C-Et-Cbz** and the material formed at the electrode, indicating that the π-conjugation is not extended (and even restricted) in the latter which is different from what is commonly observed for other linear π-systems.[47-53] This particularity can be first explained by the carbon atoms involved in the coupling. Indeed, as previously shown with various carbazole oligomers or polymer,[46] such type of anodic couplings take place at the C3 and C6 carbon atoms (as for classical electrophilic aromatic substitutions),[54] which are both in *meta* position of the biphenyl linkage leading therefore, from this point of view, to an electronic decoupling. Leclerc and coworkers have indeed reported that the oxidation of a linear poly(2,7-carbazole) leads to coupling reactions at these C3/C6 positions.[55] Secondly and considering that the carbazole units in **[4]C-Et-Cbz** are connected from their C2 and C7 positions to form the nanoring, one can suppose that linking two nanorings by their C3 and/or C6 positions would provide a sterically hindered molecular system, resulting in a perturbation of the π-electron delocalization within the nanoring and hence a lower HOMO energy level (Figure S40). Thus, we believe that both electronic and steric considerations can be invoked to understand the HOMO lowering observed for the present electrodeposited material compared to its monomer**[4]C-Et-Cbz**.

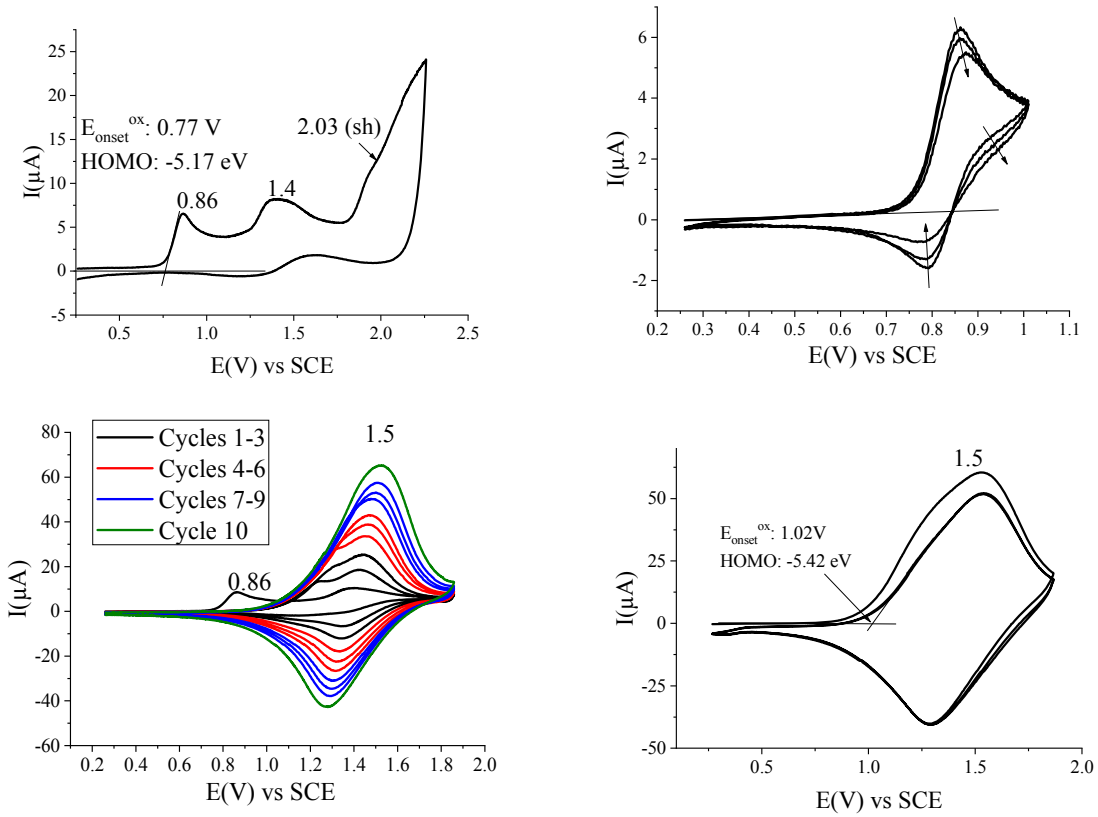

Figure 4. Cyclic voltammetry (100 mV/s) of **[4]C-Et-Cbz** [2×10^{-3} M] CH_2Cl_2/Bu_4NPF_6 (0.2 M), platinum electrode diameter 1 mm. Top left: one scan 0.25/2.25 V in CH_2Cl_2; Top right: three scans between 0.25/1 V in CH_2Cl_2; Bottom left: ten scans 0.25/1.86 V in CH_2Cl_2; Bottom right: three scans 0.27/1.86 V (modified platinum working electrode).

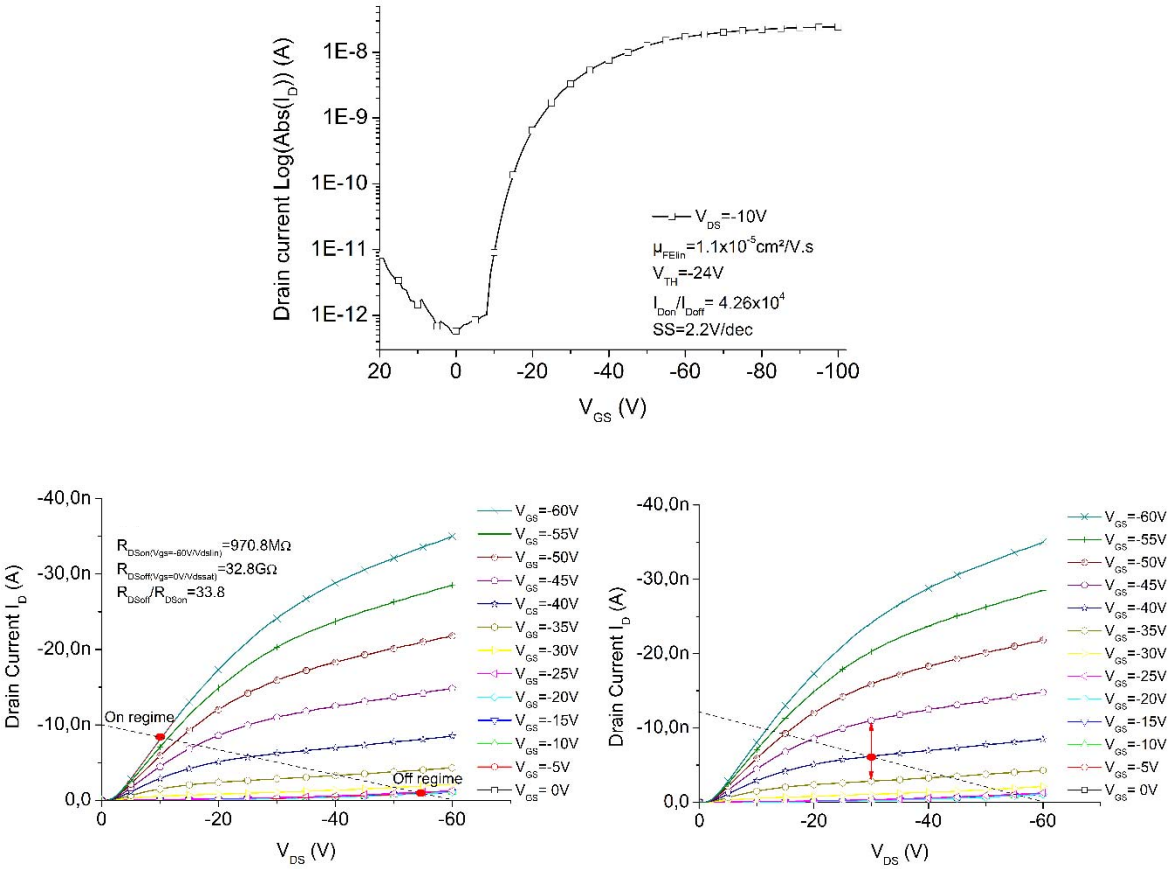

Figure 5. Top: Transfer characteristic in linear regime of OFET with V_{DS}=-10V; Bottom: Output Characteristics: (Left) OFET in digital circuit with two polarization points (On and Off regimes). (Right) OFET in analog circuit with one polarization point.

Finally, in order to determine the charge transport properties, **[4]C-Et-Cbz** has been used as active layer in p-type channel OFETs possessing a bottom-gate bottom-contact (BG-BC) architecture (device structure[56, 57] in Figure S41). This BG-BC structure, in which the active layer is evaporated in the last step, avoids any structural effect resulting from the deposition of other layers. First, it should be mentioned that **[4]C-Et-Cbz** can be easily evaporated (230°C, 2.10^{-7} mbar). OFET characterization provides a mobility μ_{FE} of 1.1 $\times 10^{-5}$ cm² $V^{-1}s^{-1}$, a threshold voltage V_{TH} of 24 V, a subthreshold swing SS of 2.2 V/dec and an on/off ratio of the drain current (I_{Don}/I_{Doff}) of 4.26 10^4, Figure 5. Despite this hole mobility being obviously low in regards to the state of the art,[58] this work displays the first incorporation of a nanoring in a non-optimized OFET and hence the first example of a transfer characteristic and a FE mobility. It is important to mention that SS (capability to switch between on and off state) is particularly

low (2.2 V/dec), translating the electrical quality of the nanoring-insulator interface. This can be advantageously used in the future.

To go deeper in the understanding of the behaviour of **[4]C-Et-Cbz** in an OFET, output characteristics have been recorded. Output characteristics constitute important data to understand OFET behaviour in an electronic circuit, which is the final goal of these components.[59, 60] Indeed, two working modes could be employed for an OFET. The first one is the use of OFETs in a digital circuit. In this case, the OFET is used in two distinct polarization points. In the 'on' regime, Gate-Source voltage V_{GS} should be high and equal to the supply voltage of the circuit ($V_{GS}=V_{DD}$) when Drain-Source voltage V_{DS} is close to 0 V. This regime is called linear regime and Drain-Source resistance R_{DS} has to be low ($R_{DS}=R_{DSon}$). In the 'off' regime, voltages are inverted with V_{GS} equal to ground value ($V_{GS}=0V$) and V_{DS} equal to the supply voltage of the circuit ($V_{DS}=V_{DD}$). This regime is called saturated regime with a high value of R_{DS} ($R_{DS}=R_{DSoff}$). In the case of a digital circuit, the R_{DSoff}/R_{DSon} ratio has to be high to discriminate the two regimes. The slopes in the saturated and linear regimes for the present case of **[4]C-Et-Cbz** are different enough ($R_{DSoff}/R_{DSon}=33.8$) to differentiate these two regimes (Figure 5, bottom-left), which is interesting for future applications.

The second working mode is the use of OFETs in an analog circuit. In this case, OFET is supplied with only one polarization point where Drain current I_D is independent of V_{DS} and a small change in V_{GS} value (small signal regime) has a high impact on I_D value. This polarization point is fixed with the crossover of output characteristics and resistance characteristics used to polarize the OFET (Figure 5, bottom-right). In the case of **[4]C-Et-Cbz**, the dependence of I_D to V_{DS} is low and we can therefore imagine using this OFET in an analog circuit to amplify small input signal. We are working in this direction. Thus, **[4]C-Et-Cbz-**based OFET displays some interesting characteristics such as a low dependence of I_D to V_{DS}.

Conclusion

To conclude, we report in this work a detailed structure-property relationship study of [4]cyclo-*N*-ethyl-2,7-carbazole **[4]C-Et-Cbz** and its first incorporation in an OFET. **[4]C-Et-Cbz** is obtained in a four-steps synthesis with an interesting yield of 22%. The structural and electronic properties have been compared to those of structurally related analogues **[4]C-diEt-CF** (with carbon bridges) and **[8]-CPP** (without any bridge) in order to shed light on the impact of the bridging in nanorings. Of particular interest, we have notably shown that **[4]C-Et-Cbz** possesses a high HOMO energy (-5.17 eV) and that the emission properties are kept in solid state (in term of wavelength and quantum yield). We believe that these appealing emission properties can be used in the future in optoelectronic devices. **[4]C-Et-Cbz** has been successfully incorporated as active layer in a p-type channel OFET with a particularly low SS of 2.2 V/dec possessing a bottom-gate bottom-contact architecture. The FE mobility extracted, 1.1×10^{-5} $cm^2.V^{-1}.s^{-1}$ appears as the first value measured for a nanoring and shows the possibility to use such macrocyles with radially directed π-orbitals in organic electronic devices increasing therefore the molecular diversity of organic semi-conductors. With a more accurate molecular design (alkyl chain engineering for example), this performance will be surely improved in the future. We are currently working in this direction. Thus, these results not only show that nanorings can be used as active layer in OFETs but also provides a first benchmark value.

Supporting Information

Supporting Information is available from the Wiley Online Library or from the author.

Acknowledgments

This project has received funding from the European Union's Horizon 2020 research and innovation program under grant agreement No 699648 (FRODO Project). This work is supported by the European Union through the European Regional Development Fund (ERDF), the Ministry of Higher Education and Research, the Région Bretagne (ARED DIADEM, FL),

the Departement d'Ille et Vilaine and Rennes Metropole, through the CPER Project 2015-2020 MATECOM-ORGAFLEX. The authors would like to thank the CINES (Montpellier N° 2018-A0040805032) for computing time, the ANR (n°14-CE05-0024) for PhD grants (LJS and FL), the CDFIX and CRMPO (Rennes) and especially Clément Orione for the variable temperature NMR studies.

Received: ((will be filled in by the editorial staff))
Published online: ((will be filled in by the editorial staff))

References

[1]R. Jasti, J. Bhattacharjee, J. B. Neaton, C. R. Bertozzi, *J. Am. Chem. Soc.* **2008**, *130*, 17646-17647.
[2]H. Omachi, Y. Segawa, K. Itami, *Acc. Chem. Res.* **2012**, *45*, 1378-1389.
[3]E. R. Darzi, R. Jasti, *Chem. Soc. Rev.* **2015**, *44*, 6401-6410.
[4]M. R. Golder, R. Jasti, *Acc. Chem. Res.* **2015**, *48*, 557-566.
[5]S. E. Lewis, *Chem. Soc. Rev.* **2015**, *44*, 2221-2304.
[6]S. Yamago, E. Kayahara, T. Iwamoto, *Chem. Rec.* **2014**, *14*, 84-100.
[7]Y. Segawa, A. Fukazawa, S. Matsuura, H. Omachi, S. Yamaguchi, S. Irle, K. Itami, *Org. Biomol. Chem.* **2012**, *10*, 5979-5984.
[8]T. Matsuno, S. Sato, R. Iizuka, H. Isobe, *Chem. Sci.* **2015**, *6*, 909-916.
[9]B. M. White, Y. Zhao, T. E. Kawashima, B. P. Branchaud, M. D. Pluth, R. Jasti, *ACS Cent. Sci.* **2018**, *4*, 1173-1178.
[10]K. Miki, K. Saiki, T. Umeyama, J. Baek, T. Noda, H. Imahori, Y. Sato, K. Suenaga, K. Ohe, *Small* **2018**, *14*, 1800720.
[11]M. Ball, Y. Zhong, B. Fowler, B. Zhang, P. Li, G. Etkin, D. W. Paley, J. Decatur, A. K. Dalsania, H. Li, S. Xiao, F. Ng, M. L. Steigerwald, C. Nuckolls, *J. Am. Chem. Soc.* **2016**, *138*, 12861-12867.
[12]J. B. Lin, E. R. Darzi, R. Jasti, I. Yavuz, K. N. Houk, *J. Am. Chem. Soc.* **2019**, *141*, 952-960.
[13]S. Canola, C. Graham, Á. J. Pérez-Jiménez, J.-C. Sancho-García, F. Negri, *Phys. Chem. Chem. Phys.* **2019**, *21*, 2057-2068.
[14]J. L. Bredas, S. R. Marder, *The WSPC References on Organic Electronics: Organic Semi-Conductors*, World Scientific
[15]Y.-Y. Liu, J.-Y. Lin, Y.-F. Bo, L.-H. Xie, M.-D. Yi, X.-W. Zhang, H.-M. Zhang, T.-P. Loh, W. Huang, *Org. Lett.* **2015**, 172-175.
[16]E. Kayahara, L. Sun, H. Onishi, K. Suzuki, T. Fukushima, A. Sawada, H. Kaji, S. Yamago, *J. Am. Chem. Soc.* **2017**, *139*, 18480-18483.
[17]V. Coropceanu, J. Cornil, D. A. da Silva Filho, Y. Olivier, R. Silbey, J.-L. Brédas, *Chem. Rev.* **2007**, *107*, 926-952.
[18]B. Wex, B. R. Kaafarani, *J. Mater. Chem. C* **2017**, *5*, 8622-8653.
[19]C. Poriel, J. Rault-Berthelot, *J. Mater. Chem. C* **2017**, *5*, 3869-3897
[20]C. Poriel, J. Rault-Berthelot, *Acc. Chem. Res.* **2018**, *51*, 1818-1830.
[21]N. Blouin, M. Leclerc, *Acc. Chem. Res.* **2008**, *41*, 1110-1119.
[22]A. C. Grimsdale, K. Müllen, *Macromol. Rapid. Commun.* **2007**, *28*, 1676-1702.
[23]L. Sicard, C. Quinton, J.-D. Peltier, D. Tondelier, B. Geffroy, U. Biapo, R. Métivier, O. Jeannin, J. Rault-Berthelot, C. Poriel, *Chem. Eur. J.* **2017**, *23*, 7719-7723.
[24]M. Romain, D. Tondelier, J.-C. Vanel, B. Geffroy, O. Jeannin, J. Rault-Berthelot, R. Métivier, C. Poriel, *Angew. Chem. Int. Ed.* **2013**, *52*, 14147-14151.
[25]M. Romain, D. Tondelier, B. Geffroy, O. Jeannin, E. Jacques, J. Rault-Berthelot, C. Poriel, *Chem. Eur. J.* **2015**, *21*, 9426–9439.

[26]S.-H. Jung, W. Pisula, A. Rouhanipour, H. J. Räder, J. Jacob, K. Müllen, *Angew. Chem. Int. Ed.* **2006**, *45*, 4685-4690.
[27]Y. Kuroda, Y. Sakamoto, T. Suzuki, E. Kayahara, S. Yamago, *J. Org. Chem.* **2016**, *81*, 3356-3363.
[28]S. Yamago, Y. Watanabe, T. Iwamoto, *Angew. Chem. Int. Ed.* **2010**, *49*, 757-759.
[29]S. Hitosugi, W. Nakanishi, T. Yamasaki, H. Isobe, *Nat. Commun.* **2011**, *2*, 492.
[30]L. Sicard, O. jeannin, J. Rault-Berthelot, C. Quinton, C. Poriel, *Chem. Plus Chem.* **2018**, *83*, 874-880.
[31]Z. Sun, P. Sarkar, T. Suenaga, S. Sato, H. Isobe, *Angew. Chem Int. Ed.* **2015**, *54*, 12800-12804.
[32]J. Xia, J. W. Bacon, R. Jasti, *Chem. Sci.* **2012**, *3*, 3018.
[33]X. M. Duan, L. G. Chen, Y. J. Xu, Y. Li, J. Han, L. P. Li, *Acta Crystallog. E* **2004**, *60*, o1931-o1932.
[34]C. Ramathilagam, N. Venkatesan, P. Rajakumar, P. R. Umarani, V. Manivannan, *Acta Crystallog. E* **2011**, *67*, o2796.
[35]E. Asker, J. Masnovi, *Acta Crystallog. E* **2004**, *60*, o1613-o1615.
[36]A. Bondi, *J. Phys. Chem.* **1964**, *68*, 441-451.
[37]M. Fujitsuka, D. W. Cho, T. Iwamoto, S. Yamago, T. Majima, *Phys. Chem. Chem. Phys.* **2012**, *14*, 14585-14588.
[38]C. Graham, M. Moral, L. Muccioli, Y. Olivier, Á. J. Pérez-Jiménez, J.-C. Sancho-García, *Int. J. Quantum Chem* **2018**, *118*, e25562.
[39]Y. Segawa, A. Kukazawa, S. Matsuura, H. Omachi, S. Yamaguchi, S. Irle, K. Itami, *Org. Biomol. Chem.* **2012**, *10*, 5979-5984.
[40]L. Adamska, I. Nayyar, H. Chen, A. K. Swan, N. Oldani, S. Fernandez-Alberti, M. R. Golder, R. Jasti, S. K. Doorn, S. Tretiak, *Nano Letters* **2014**, *14*, 6539-6546.
[41]T. Iwamoto, Y. Watanabe, Y. Sakamoto, T. Suzuki, S. Yamago, *J. Am. Chem. Soc.* **2011**, *133*, 8354-8361.
[42]S. Mallick, S. Maddala, K. Kollimalayan, P. Venkatakrishnan, *J. Org. Chem* **2019**, *84*, 73-93.
[43]P. Hapiot, C. Lagrost, F. Le Floch, E. Raoult, J. Rault-Berthelot, *Chem. Mater.* **2005**, *17*, 2003-2012.
[44]R. J. Fenn, K. W. Krantz, J. D. stuart, *J. Electrochem. Soc.* **1976**, 1643-1647.
[45]R. Qin, Z. Bo, *Macromol. Rapid Commun.* **2012**, *33*, 87-91.
[46]K. Karon, M. Lapkowski, *J. Solid State Electrochem.* **2015**, *19*, 2601-2610.
[47]J. Roncali, *Chem. Rev.* **1992**, *92*, 711-738.
[48]J. Simonet, J. Rault-Berthelot, *Prog. Solid State Chem.* **1991**, *21*, 1-48.
[49]C. Poriel, J. Rault-Berthelot, D. Thirion, *J. Org. Chem.* **2013**, *73*, 886-898.
[50]J. Rault-Berthelot, C. Poriel, F. Justaud, F. Barrière, *New J. Chem.* **2008**, *32*, 1259-1266.
[51]C. Poriel, Y. Ferrand, P. Le Maux, J. Rault-Berthelot, G. Simonneaux, *Synth. Met.* **2008**, *158*, 796-801.
[52]C. Poriel, J.-J. Liang, J. Rault-Berthelot, F. Barrière, N. Cocherel, A. M. Z. Slawin, D. Horhant, M. Virboul, G. Alcaraz, N. Audebrand, L. Vignau, N. Huby, G. Wantz, L. Hirsch, *Chem. Eur. J.* **2007**, *13*, 10055-10069.
[53]C. Poriel, Y. Ferrand, P. Le Maux, C. Paul-Roth, G. Simonneaux, J. Rault-Berthelot, *J. Electroanal. Chem.* **2005**, *583*, 92-103.
[54]S.-i. Kato, H. Noguchi, A. Kobayashi, T. Yoshihara, S. Tobita, Y. Nakamura, *J. Org. Chem* **2012**, *77*, 9120-9133.
[55]G. Zotti, G. Schiavon, S. Zecchin, J.-F. Morin, M. Leclerc, *Macromolecules* **2002**, *35*, 2122-2128.
[56]J.-D. Peltier, B. Heinrich, B. Donnio, O. Jeannin, J. Rault-Berthelot, E. Jacques, C. Poriel, *J. Mater. Chem. C* **2018**, *6*, 13197-13210.
[57]J.-D. Peltier, B. Heinrich, B. Donnio, E. Jacques, J. Rault-Berthelot, C. Poriel, *ACS Appl. Mater. Interfaces* **2017**, *9*, 8219-8232.
[58]J. T. E. Quinn, J. Zhu, X. Li, J. Wang, Y. Li, *J. Mater. Chem. C* **2017**, *5*, 8654-8681.
[59]Y. Xu, C. Liu, D. Khim, Y.-Y. Noh, *Phys. Chem. Chem. Phys.* **2015**, *17*, 26553-26574
[60]M. Romain, M. Chevrier, S. Bebiche, T. Mohammed-Brahim, J. Rault-Berthelot, E. Jacques, C. Poriel, *J. Mater. Chem. C* **2015**, *3*, 5742-5753.